Vibrational properties of the layered semiconductor germanium sulfide under hydrostatic pressure: Theory and experiment

H. C. Hsueh, M. C. Warren, H. Vass, G. J. Ackland, S. J. Clark, and J. Crain

Department of Physics and Astronomy, The University of Edinburgh, Edinburgh, EH9 3JZ, Scotland, United Kingdom

(Received 31 July 1995; revised manuscript received 10 January 1996)

The structural and vibrational properties of the prototypical layered semiconductor germanium sulfide (GeS) have been studied under pressure using a combination of high-resolution x-ray powder diffraction, Raman scattering, and *ab initio* simulation. The theoretically and experimentally determined pressure response of the static and dynamical properties are in good agreement with each other. No structural phase transformation is found up to 94 kbar. Inspection of the calculated eigenvectors of zone center phonons at several pressures indicates that the validity of the rigid-layer mode approximation is appropriate only at near-ambient pressure conditions and breaks down under compression. [S0163-1829(96)00122-1]

I. INTRODUCTION

Quasi-two-dimensional layered compounds have been the subject of sustained interest for many years because of the coexistence of weak interlayer and stronger intralayer interactions. Understanding the bonding in layered solids is important especially in view of potential applications of these materials as lubricants and in intercalation compounds. The vibrational properties of these highly anisotropic materials have been the focus of particular attention because they provide the most direct measure of the disparity in the force constants responsible for cohesion.

A characteristic feature of the lattice dynamics of anisotropic solids is the existence of "rigid-layer" (RL) vibrations. These very low-frequency optical phonons were first identified by Zallen *et al.* in layered chalcogenide crystals[1] and they correspond to a displacement pattern in which the layers move relative to each other as rigid units. The restoring force responsible for the RL mode is due to the interlayer coupling: very weak coupling implies very low RL mode frequencies and a frequency separation between inter- and intralayer modes.

The weakness of the interlayer coupling in layered solids makes the vibrations amenable to symmetry considerations based on factor-group analysis of two-dimensional (diperiodic) symmetry groups (DG).[2,3] In the limiting case of zero interlayer coupling, Raman- and infrared-active vibrations will exist as degenerate pairs. This degeneracy is lifted by the presence of a weak interlayer interaction. This situation is analogous to Davydov splitting in molecular crystals.[4] Therefore, a fairly good quantitative estimation of the weak interlayer interaction can be made by careful measurement of the Raman-infrared splitting.[3,5,6]

It is expected that pressure will have the effect of preferentially enhancing the interlayer coupling and that it will have a dramatic effect on the crystal structure and the RL vibrations. Despite the evident importance of understanding pressure effects in highly anisotropic solids, there have been relatively few studies reported. Crystallographic studies are hindered by the fact that the layered structures are generally complex and require the determination of atom positions un-

der pressure for complete characterization. Vibrational studies are complicated by the fact that RL vibrations exist at very low frequencies and are easily obscured by scattered light. This makes high-pressure diamond-anvil cell studies particularly challenging. Also, spectroscopic studies provide no information regarding phonon eigenvectors, therefore the validity of the RL mode approximation cannot be assessed on the basis of such measurements. The exploration of this is a partial motivation for this work.

The complexity of layered structures has also generally limited theoretical treatments to phenomenological valence force models of lattice dynamics.[7] Such empirical calculations have been applied to GeS and the phonon dispersion relation for GeS has been calculated in this way.[8] A related linear-chain model was also used to analyze the lattice vibrations of several other layered compounds.[9–11]

The pressure dependence of the Raman spectrum of the isostructural semiconductors GeS and GeSe has been studied up to 7 kbar using a hydrostatic pressure bomb[12] and it was found that the normal mode frequencies increase linearly over this relatively low-pressure range. The large difference between the pressure coefficients of RL and intralayer modes shows that the Grüneisen approximation does not apply to these materials. This anomalous phenomenon has also been found in the other layered and molecular crystals.[4,13] In order to extend the Grüneisen approximation to solids characterized by a hierarchy of forces, Zallen[13] introduced a more general empirical vibrational scaling law in which the bond-stiffness–bond-length is used to replace the volume of the unit cell as the scaling parameter.

A very recent study of the anisotropic properties of the layered semiconductor germanium selenide[14] (GeSe) under compression showed that the layered structure was stable up to at least 130 kbar and that a pressure-induced closure of the band gap of GeSe is responsible for the observed metallization transition.[15] The structural response was also studied in this work and it was found that the compression mechanism (pressure dependence of unit cell and atom positions) was well accounted for by *ab initio* calculations.

However, frozen-phonon calculations of the rigid-layer shear mode frequency substantially overestimated the experimentally observed mode frequency.[16] This overestimate be-

came larger with increasing pressure. It was suggested that the discrepancy was due to the failure of the RL approximation at elevated pressure. Under such circumstances, the frozen-phonon method for determining vibrational frequencies would be inappropriate.

There is therefore a strong motivation to explore theoretically the pressure dependent vibrational properties of anisotropic solids in a way which does not rely on the validity of the RL approximation. The objective of this paper is to present a detailed account of the structural and vibrational properties of the prototypical layered semiconductor GeS under hydrostatic pressure and to assess the degree to which the RL mode approximation holds under compression. In the present work we apply both high-sensitivity experiments and first-principles computer simulation in order to address these issues.

The paper is organized as follows. The structural details of GeS are given in Sec. II. The high-pressure experimental methods are outlined in Sec. III. The overall features of the theoretical *ab initio* calculation are given in Sec. IV. The observations of structural and dynamical properties of GeS are described in Sec. V. The details of the breakdown of the RL approximation are discussed in Sec. VI and we summarize this work in Sec. VII.

II. STRUCTURAL DETAILS OF GERMANIUM SULFIDE

Germanium sulfide adopts a double-layered orthorhombic structure with the $Pcmn$ (D_{2h}^{16}) spacegroup at ambient pressure. Choosing the c axis to be normal to the plane of layers, the unit cell parameters are $a = 4.30$ Å, $b = 3.65$ Å, and $c = 10.44$ Å.[17] Two free atomic positional parameters (u and v) for Ge and S atoms characterize the structure completely and each species of atom is located at positions (u_{Ge}, 1/4, v_{Ge}) and (u_S, 1/4, v_S). The crystal structure of GeS is illustrated in Fig. 1.

The unit cell contains two double layers and each double layer is formed by covalently bonded Ge-S pairs in which atoms are threefold coordinated inside the double layer. However, the interlayer coupling is weak and this is responsible for the observed easy cleavage of the GeS crystal perpendicular to the c axis.

At ambient pressure, there are two distinct bond lengths. We denote the bond nearly parallel to the crystallographic c axis as the C bond and the bond in the a-b plane as an AB bond. We also define the interlayer distance as $2v_{Ge}c$ (Ref. 14) to examine the structural properties under pressure. These designations will be useful in describing the pressure-induced structural response.

III. EXPERIMENTAL METHODS

A. Angle-dispersive powder x-ray diffraction

High-pressure structural studies were carried out at station 9.1 of the Synchrotron Radiation Source at Daresbury Laboratory using powder x-ray diffraction and an image plate area detector. A detailed description of the experimental apparatus can be found elsewhere.[18] In view of the layered character and preferential cleavage direction of this material, care was taken to produce a uniform powder so as to limit preferred orientation. In order to obtain a fine powder of the
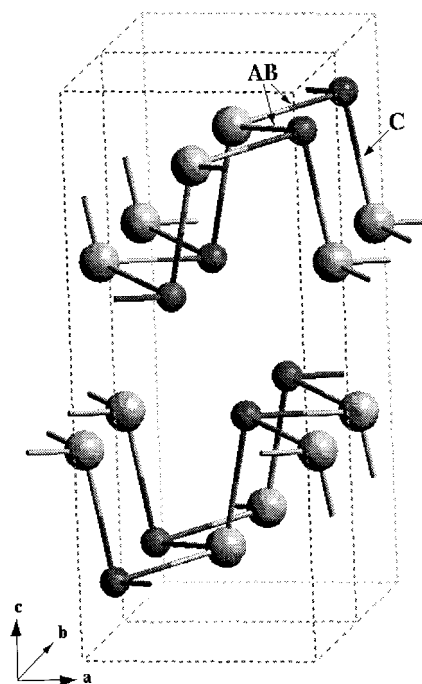
FIG. 1. Illustration of the GeS structure showing the threefold covalent coordination in the layers. Ge and S are represented as small and big spheres, respectively. The C bond and the AB bond are identified. Two unit cells are shown (doubled along the b crystallographic axis). The plane of the layers is perpendicular to the c axis.

layered GeS material a single-crystal sample was first crushed and then placed in pure ethanol. The finest particles (grain size <5 μm), those which remained suspended in the alcohol, were then placed in a Merrill-Bassett diamond anvil pressure cell along with a 4:1 methanol-ethanol mixture and a chip of ruby for pressure calibration. The incident beam was collimated to a diameter of 75 μm and the distance between the sample and the image plate was approximately 300 mm. Exposure times were approximately 4 h in length. A wavelength of 0.4447 Å was used for all measurements. Data analysis was done using the Platypus software package[19] for pattern for integration of the two-dimensional image and subsequent Reitveld refinement using the MPROF program.[20]

B. Raman scattering

Vibrational spectra were obtained using Raman spectroscopy on single-crystal samples. The 6764 Å line of a Kr$^+$ laser was used as the excitation source. The laser power was estimated to be 90 mW at the sample. A Coderg T-800 triple grating spectrometer was used to collect spectra and the slit size was set at 400 μm which gave a resolution of approximately 1.5 cm^{-1}. As in the x-ray experiments, pressure-Raman measurements were performed with a 4:1 mixture of methanol-ethanol as the transmitting fluid and pressure was determined using the ruby fluorescence scale. Tungsten gaskets were preindented to a diameter of 0.2 mm and used with low fluorescence 0.6 mm culet diamonds for all measurements. Spectra were collected in backscattering geometry

normal to the c axis of the crystal using a count time of 20 s per data point. In order to minimize stray light and optimize the important low-frequency portion of the spectra a lens having a small focal length was placed between the mirror and sample. This gave a very tightly focused spot on the sample and a relatively defocused beam in the diamonds. Contamination from air spectra was reduced by flushing the entire sample chamber with argon and emission lines were eliminated by prism filters and an iris.

Low-temperature data were collected using a CTI Cryogenics closed-cycle cryostat and a Lakeshore Cryogenics temperature controller. The sample was firmly affixed to a copper backing plate which made thermal contact with the sample. Temperature control was better than 0.1 K. The scattering geometry and instrumental resolution were identical to the high-pressure arrangement.

IV. COMPUTATIONAL DETAILS

A. Electronic structure algorithm

The calculations were performed using the *ab initio* pseudopotential technique. The local density approximation (LDA) based on the Perdew-Zunger parametrization[21] was employed to describe the electronic exchange-correlation interactions. We used the Kleinman-Bylander form[22] for the nonlocal ionic pseudopotentials which were generated by the Q_c tuning method.[23,24] We used a preconditioned conjugate gradient scheme to minimize the total energy and also conjugate gradients to relax the ions under the influence of the Hellmann-Feynman forces. The plane wave basis set is expanded to an energy cutoff $\mathcal{E}_{\text{cutoff}}$ of 300 eV where we find total energies to be converged to better than 0.1 meV/cell.

To implement the Brillouin zone (BZ) integration, eight special k points were used which correspond to the $4 \times 4 \times 4$ grid in the scheme of Monkhorst and Pack[25] where we find total energies to be fully converged. The charge density was symmetrized to reflect the D_{2h}^{16} group of the GeS structure at each step in the calculation which also enforced the correct symmetry of the Hellmann-Feynman forces.

B. Unit cell optimization

Rather than make an exhaustive search of each lattice parameter, an automatic method of unit cell relaxation was used to optimize the cell dimensions under compression. The stresses on the unit cell were calculated from first principles, and used to relax the lattice parameters to their equilibrium values. A matrix h can be formed by the unit cell vectors, $\{\mathbf{a},\mathbf{b},\mathbf{c}\}$, and then a tensor $g = h^T h$. We define the N atoms to have fractional coordinates $\mathbf{s}_i$ and masses m_i (thus their Cartesian positions are $\mathbf{r}_i = h\mathbf{s}_i$). We have modified the Lagrangian of Wentzcovitch[26] to compensate for the change in basis set which occurs when the unit cell dynamics is implemented, which, like the Parrinello-Rahman Lagrangian,[27] gives the unit cell a fictitious ''boxmass'' W. To implement this, a further tensor $f_0 = (\sigma_0^T \sigma_0)$ is created from the initial cell faces where $\sigma_0 = (\mathbf{b}_0 \times \mathbf{c}_0, \mathbf{c}_0 \times \mathbf{a}_0, \mathbf{a}_0 \times \mathbf{b}_0)$ such that the Lagrangian takes the form

$$\mathcal{L} = \sum_{i=1}^{N} \frac{m_i}{2} \dot{\mathbf{s}}_i^T \cdot g\, \dot{\mathbf{s}}_i - U(\{\mathbf{r}_i\}) + \frac{W}{2}\text{Tr}(\dot{h} f_0 \dot{h}^T) - P\Omega, \quad (1)$$

where P is an external isotropic pressure and Ω the volume of the simulation cell. This generates an equation of motion containing the *ab initio* stress tensor Π:

$$\ddot{h} = \frac{1}{W}(\Pi - P)\sigma f_0^{-1}, \quad (2)$$

which is integrated using the standard Verlet algorithm, with an adjustable time step which is chosen along with W such that the energy minimization algorithm is stable.

However, as the cell vectors change, the plane wave basis set also changes. The number of plane waves is held constant, as this conserves the total electronic charge, but this results in a variation of the energy of the highest plane wave kinetic energy. The effect of this is that the cutoff energy $\mathcal{E}_{\text{cutoff}}$ changes. Since it is physically preferable to keep the cutoff fixed[28] a Pulay correction[29] Π_P is added to the stress to compensate for this effect:[30]

$$\Pi_P = \frac{2}{3\Omega} \frac{\partial E}{\partial \ln \mathcal{E}_{\text{cutoff}}}, \quad (3)$$

thus $\Pi = \Pi_P + \Pi_{\text{calc}}$. Calculating the Pulay correction is a straightforward process: the total energy $E(\mathcal{E}_{\text{cutoff}})$ of a fixed configuration (box and ionic positions) is found for a number of different cutoff energies; the differential term in this equation is then approximated from a fit to these total energies. The Pulay correction was found to be -20.25 kbar for GeS around $\mathcal{E}_{\text{cutoff}} = 300$ eV.

A quenched molecular dynamics scheme was used to find equilibrium lattice parameters. In this method simultaneous ionic and unit cell relaxation is possible. We find that faster convergence is achieved by alternately relaxing the unit cell and structural parameters because of the strong coupling between ionic and unit cell degrees of freedom. We relax the pressure until the stresses (including the Pulay correction) are below 0.001 eV/Å^3, and ionic relaxation continues until no force component exceeded 0.005 eV/Å. It is important to note that accurate ionic and cell relaxation is essential for reliable lattice dynamics calculations.

C. Phonon frequency calculations

The zone-center phonons of GeS were calculated in two ways. First, a dynamical matrix diagonalization method was implemented within the harmonic approximation and second, we perform frozen-phonon calculations to obtain the theoretical rigid-layer frequencies.

We calculate the full dynamical matrix as follows: the force constants of a crystal relate the displacements of the ions from their equilibrium positions to the resulting forces. If the κth ion in the lth unit cell has displacement $\mathbf{u}_{l\kappa}$ from an equilibrium position $\mathbf{x}_{l\kappa}$, then the forces on the ions are given by

$$\mathbf{F}_{l\kappa} = \mathbf{\Phi}_{l\kappa l'\kappa'}\mathbf{u}_{l'\kappa'}, \quad (4)$$

where $\mathbf{\Phi}$ are the harmonic force constants. In order to find the phonon frequencies and eigenvectors at some wave vector, the Fourier transformed dynamical matrix must be formed, consisting of the force constants scaled by ionic masses:

TABLE I. Observed and calculated structural parameters for GeS at ambient conditions. The units for cell dimensions (a, b, and c) are in Å and those for the positional parameters are in fractional coordinates.

	a	b	c	u_{Ge}	v_{Ge}	u_S	v_S
Calc. [a]	4.184	3.556	10.123	0.123	0.117	0.499	-0.148
Expt. [a]	4.305	3.643	10.495	0.119	0.123	0.499	-0.165
Expt. [b]	4.30	3.65	10.44	0.106	0.121	0.503	-0.148
Expt. [c]	4.30	3.64	10.47	0.127	0.122	0.499	-0.151

[a]Present work.
[b]Reference 17.
[c]Reference 40.

$$D_{\alpha\beta}(^{\mathbf{q}}_{\kappa\kappa'})= \frac{1}{\sqrt{m_\kappa m_{\kappa'}}}\sum_l \phi_{0\kappa_\alpha l\kappa'_\beta}\exp(i\mathbf{q}\cdot[\mathbf{x}_{l\kappa'}-\mathbf{x}_{0\kappa}]).$$
$$(5)$$

At each wave vector $\mathbf{q}$, the dynamical matrix is diagonalized to give eigenvalues $(-\omega^2)$ and phonon eigenvectors in normalized mass-reduced coordinates $\epsilon_i=\sqrt{m_i}u_i$.

However, if only the zone-center phonons are required, then only one unit cell needs to be simulated. The elements of $\mathbf{D}(^0_{\kappa\kappa'})$ were thus found from the Hellmann-Feynman forces generated when the (κ')th ion is displaced a small amount ξ from equilibrium along β:

$$D_{\alpha\beta}(\kappa\kappa')=\frac{1}{\sqrt{m_\kappa m_{\kappa'}}}\frac{F_{\alpha\kappa}}{\xi}.$$
$$(6)$$

When complete, this matrix is then diagonalized to find the zone-center phonons.

It is also useful to use the point group symmetry of the structure to reduce the number of displacements required. If a symmetry element $\{\mathbf{S}|\mathbf{u}\}$ maps ion j to J and κ to K, then it can be shown[31] that

$$\mathbf{\Phi}_{JK}=\mathbf{S}\mathbf{\Phi}_{j\kappa}\mathbf{S}^T.$$
$$(7)$$

Hence only a subset of the possible $3N$ distortions need be performed. The remaining elements were deduced by using the transformation matrices of the point group according to (7). The frequencies and eigenvectors of the Γ modes were thus obtained from first principles.[32]

In the specific case of GeS which is orthorhombic (three distinct directions), only three independent movements of each species of atom are, in principle, needed in order to construct all the elements in the dynamical matrix when full advantage is taken of symmetry according to the methodology outlined in the above theoretical discussion. In practice, however, it is necessary to determine an appropriate magnitude of displacement in order to ensure that the harmonic approximation is satisfied. In order to test this, we make positive and negative displacements about the equilibrium positions. When the restoring forces are equal in magnitude but opposite in direction we are in the harmonic regime. In order to minimize the effects of numerical noise we chose the largest value of the displacement for which this criterion holds. We found this to be 0.005 in fractional coordinates. Diagonalization of the resulting dynamical matrix provides the eigenvalues and eigenvectors of the Γ-point modes of the

structure. In principle, arbitrary wave-vector modes can be obtained by using a superlattice calculation.

We also performed a frozen-phonon calculation to obtain the RL phonon frequencies. Instead of building up the dynamical matrix, the frozen-phonon method assumes the double layers of GeS shift rigidly and the rigid-layer eigenvector displacement patterns are used for three independent directions. The fractional displacement of the layers was also chosen to be 0.005 in order to guarantee the calculation was in the harmonic regime.

Although these optimized first-principles methods substantially reduce the computational cost, the calculations of structural relaxation and dynamical matrix construction are still expensive, requiring about 20 days of CPU time on an Alpha-AXP workstation for each pressure.

V. RESULTS

A. Structural properties

The values of the calculated equilibrium unit cell and structural parameters are presented in Table I. Also shown are the experimental results at room temperature. As is evident from Table I, the calculated lattice constants are about 2–3 % smaller than the observed room temperature results. This underestimate is attributed to the combined effect of thermal expansion (which we expect to be relatively minor) and the well-known tendency of the LDA to overbind structures.

The bond lengths and bond angles can be determined from the information contained in Table I. The calculated Ge-S bond lengths are 2.430 and 2.401 Å for bonds approximately normal to the c axis (C bonds) and for those in the a-b plane (AB bonds), respectively. The experimental values for these bond lengths are 2.457 and 2.497 Å, respectively.[17] The nearest nonbonded separation between atoms in different layers is 3.112 Å between different species and 3.138 Å between the same species according to our calculations. The experimental values for these separations are 3.286 and 3.247 Å, respectively.[17] Examination of the calculated valence charge density indicates that atoms within a given double layer are threefold coordinated via covalent bonds. There is negligible electron concentration between the layers which is a further indication that the structure is highly anisotropic.

The calculated total energy as a function of pressure is shown in Fig. 2. The points on the curve were obtained after relaxation of unit cell dimensions and internal free positional parameters. The curve therefore determines the calculated
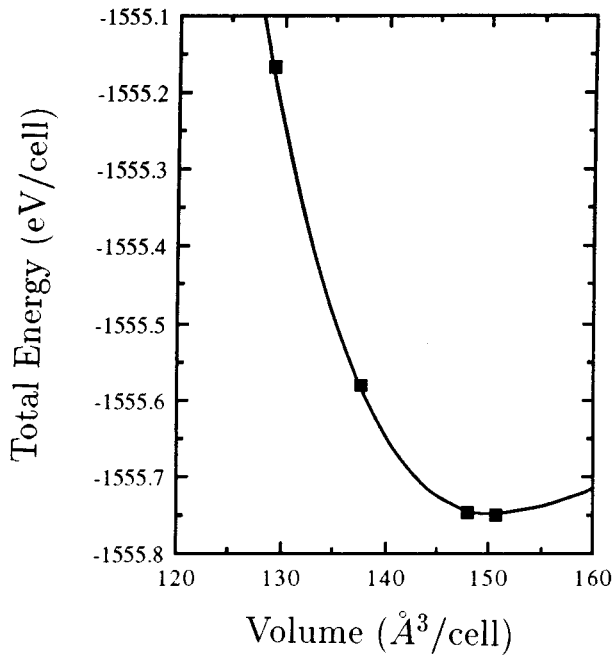
FIG. 2. Total energy vs pressure for GeS. The hydrostatic pressure response was determined by relaxation of the unit cell parameters under the influence of stresses by the procedure described in the text. Internal ionic positional parameters were relaxed by minimizing Hellmann-Feynman forces. The solid line is a third-order polynomial fit to the total energy vs unit cell volume which is included as a guide to the eye. Note that no negative pressure points are necessary to bound the minimum since constant pressure dynamics at 0 GPa is guaranteed to be the minimum.

hydrostatic response of the structure. The relaxed configuration at each point is used as the equilibrium structure for the subsequent lattice dynamical calculations.

To determine the structural response to pressure experimentally, we performed high-pressure angle-dispersive powder x-ray diffraction measurements in order to compare to our *ab initio* calculation. The diffraction data at ambient pressure and 94 kbar are shown in Fig. 3. Both the experimental and the computational results reveal that the orthorhombic layered structure remains stable up to at least 94 kbar which is consistent with previous energy dispersive x-ray diffraction investigations.[33]

The dependence of the three lattice constants of GeS as a function of hydrostatic pressure as determined by high-resolution x-ray powder diffraction and first-principles calculation is shown in Fig. 4. At 100 kbar, the calculated fractional compression of three lattice parameters a, b, and c is 0.926, 0.971, and 0.953, respectively. Like GeSe, the a axis of GeS is more compressible than either the b or c axes under pressure despite the fact that the layer planes are normal to the c axis. The dominant compression mechanism is found to be due to the bending of intralayer bonds along the a-axis direction. The calculated interlayer distance is also shown in Fig. 4 and the fractional compression of interlayer distance is 0.897 at 100 kbar. This indicates that the interlayer distance is most sensitive to pressure.

The calculated pressure dependence of the internal positional parameters, u_{Ge}, v_{Ge}, u_S, and v_S is shown in Figs.
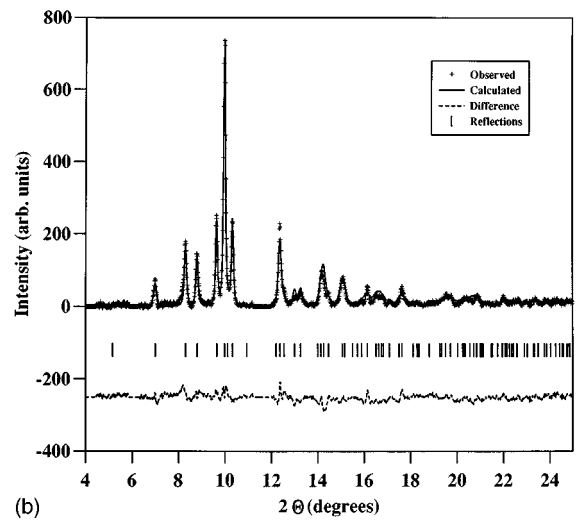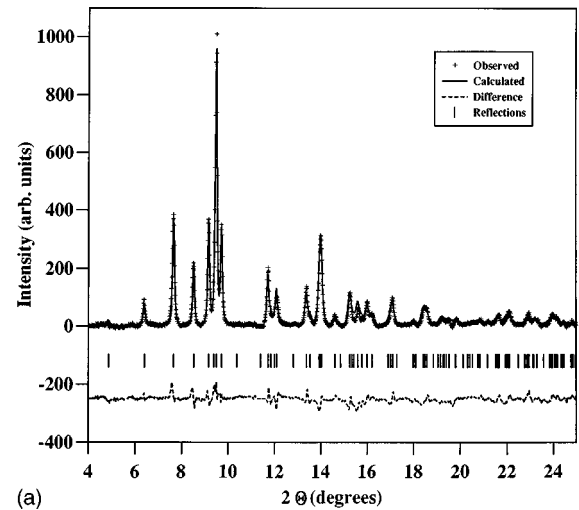
FIG. 3. Rietveld refinements of powder patterns of GeS obtained at (a) ambient pressure and (b) 94 kbar. A correction for preferred orientation along (00l) has been applied for both refinements. The wavelength of the incident beam was 0.4447 Å and the exposure time for each pattern was approximately 4 hours.

5(a)–5(d), respectively. The variation of the structural parameters of GeS with pressure is very similar to the pressure response of the structural parameters found for GeSe which has been presented in an earlier paper.[14]

At 50 kbar, the calculated bond lengths are 2.418 Å for the C bond and 2.375 Å for the AB bonds. The shortest interlayer atomic separations are calculated to be 2.964 and 2.942 Å. Thus, even at 50 kbar the material is characterized by highly anisotropic bonding and in the next section we examine the consequences of this structural anisotropy on the vibrational properties.

B. Dynamical properties

1. Ambient pressure lattice dynamical properties

The lattice vibrations of GeS are characterized by 24 zone-center modes since there are eight atoms in the primi-
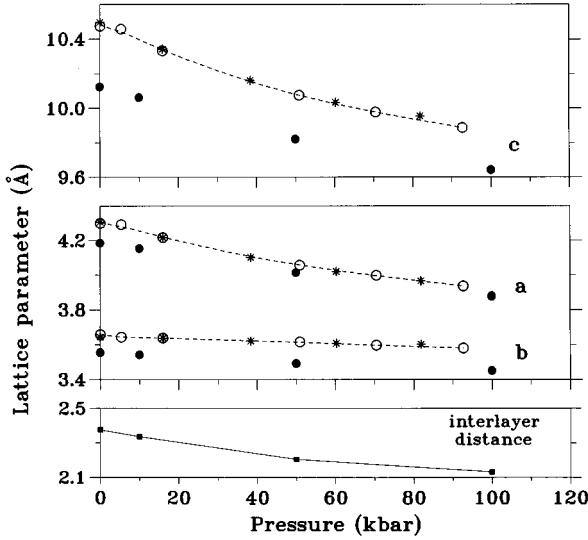
FIG. 4. Pressure dependence of GeS lattice parameters. Cell parameters refined from high-resolution powder x-ray diffraction data collected using monochromatic synchrotron radiation and an image-plate area detector are shown as open circles and star symbols (corresponding to two different sample loadings). The results of first-principles density functional theory pseudopotential calculations are also shown as solid circles. The dashed line through the experimental data is a guide to the eye. The pressure dependence of the calculated interlayer distance (see text for definition) is indicated by solid squares.

FIG. 5. Calculated pressure dependence of the internal structural parameters of GeS up to 100 kbar. The four structural parameters u_{Ge}, v_{Ge}, u_S, v_S are shown in (a), (b), (c), and (d), respectively.

tive unit cell. Apart from three acoustic vibrations, the remaining 21 optical modes can be factorized into 12 Raman-active, 7 infrared-active, and 2 inactive modes by group theory analysis of the spacegroup D_{2h}^{16}. According to DG analysis, an isolated GeS double layer exhibits 12 vibrational modes. The correlation diagram between the two groups and the activity of each of the zone-center modes are shown in Fig. 6.

The 24×24 dynamical matrix was constructed from displacements of the calculated ambient pressure structure of GeS about the equilibrium positions. Diagonalization of the matrix resulted in determination of 24 eigenfrequencies. Three of these frequencies were approximately zero and were attributed to the three acoustic modes. The remaining 21 vibrational frequencies could be grouped according to frequency. The three lowest frequencies obtained were 52.3 cm^{-1}, 64 cm^{-1}, and 77.5 cm^{-1}. Six more modes were obtained having somewhat higher frequencies ranging from approximately 88 cm^{-1} to 133 cm^{-1}. The remaining modes all had considerably higher frequencies ranging from 210 cm^{-1} to 319 cm^{-1}.

In order to obtain detailed information regarding the nature of the displacements giving rise to these frequencies we examined the corresponding eigenvectors for each of the modes. The displacement pattern associated with the lowest-frequency mode was found to correspond to a mode in which the double layers slide over each other in the crystallographic a direction. The second lowest frequency was also associated with a shear motion along the b direction. The third lowest-frequency mode was found to correspond to a compressional displacement pattern in which the layers vibrate against each
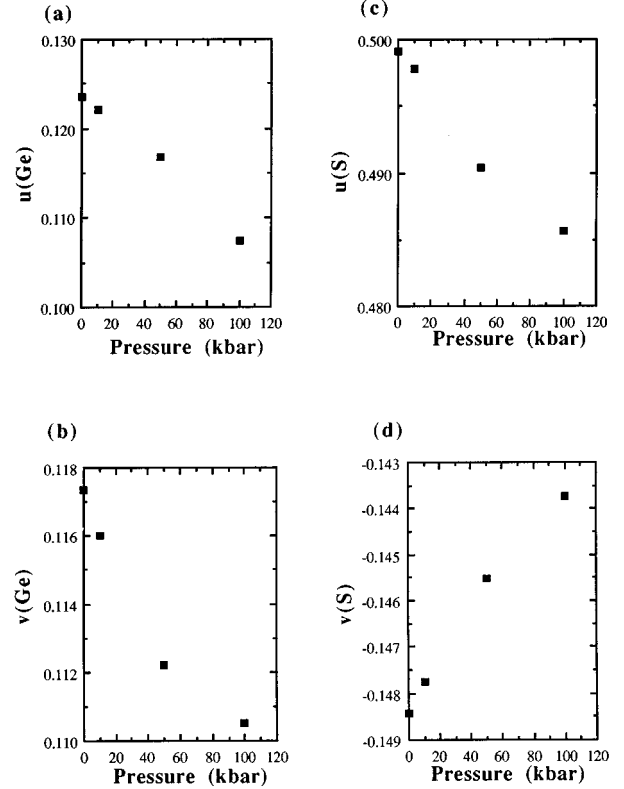
other along the c axis of the crystal. Thus the three lowest-frequency modes are clearly of nearly pure RL type under ambient conditions. The displacement patterns corresponding to the a and c directions are shown in Fig. 7. The second group of modes (in the midfrequency range) were found to arise from bond-bending vibrations and the highest-frequency vibrations were associated with displacement patterns involving covalent bond length changes.

In order to be more quantitative regarding mode assignments we have attempted to deduce the symmetry labels of all zone-center modes. The general strategy for doing this was as follows. We applied all point group symmetry operations of the structure to the set of calculated displacement eigenvectors for a given vibrational mode. We then determined the set of group characters for the vibration and were able to assign each mode to one of the irreducible representations of the $mmm(D_{2h})$ point group.[34] From this procedure[35] and the character table for the group we determined that the zone-center vibrational modes transform according to

$$\Gamma_{vib} = 4A_g + 2A_u + 2B_{1g} + 3B_{1u} + 4B_{2g} + 1B_{2u} + 2B_{3g}$$
$$+ 3B_{3u} \qquad (8)$$

(in the Mulliken notation) in which three lowest-frequency modes transform according to A_g, B_{3g}, and B_{2g} representa-
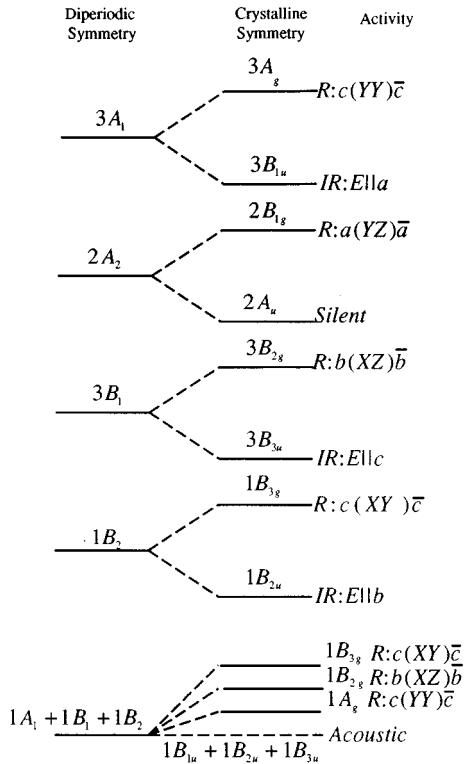
FIG. 6. Symmetry assignments, spectroscopic activities, and polarization selection rules for zone-center vibrations of the layered GeS structure. To the left of the figure is shown the symmetry labels for diperiodic group symmetry which are appropriate for the case in which there is no interlayer coupling (Ref. 6). The abbreviations R and IR represent Raman- and infrared-active modes, respectively.

tions, respectively. This is consistent with previous symmetry assignments of the vibrations.[6]

At ambient pressure, both the low-temperature and the room temperature Raman spectra were measured and the results of our measurements are shown in Fig. 8. The lowest-frequency modes we detect in our experiment occur at 48 cm^{-1} (A_g shear mode) and 56 cm^{-1} (B_{3g} shear mode) at room temperature and 52 cm^{-1} (A_g shear mode) at 10 K, respectively. These values are in excellent agreement with the calculated results for these modes. Our experimental values for the Raman-active mode frequencies agree well with those presented in earlier papers at both room temperature and low temperature for all modes which were accessible in our experimental geometry. However, since we perform only $c(XY)\bar{c}$ scattering the B_{2g} compressive mode is inaccessible in our measurements. This mode has been measured previously at both room temperature and 20 K,[36] and it is located at approximately 75.5 cm^{-1} at 300 K and 76.5 cm^{-1} at 20 K which is also in close agreement with our calculated value of 77.5 cm^{-1}. A summary of the experimental and calculated results for the ambient pressure vibrational properties is given in Table II. It is evident that the mode frequencies increase with decreasing temperature as shown in Table II. Since our calculations are performed for $T=0$, the low-temperature data provide the most appropriate comparison to our calculations.
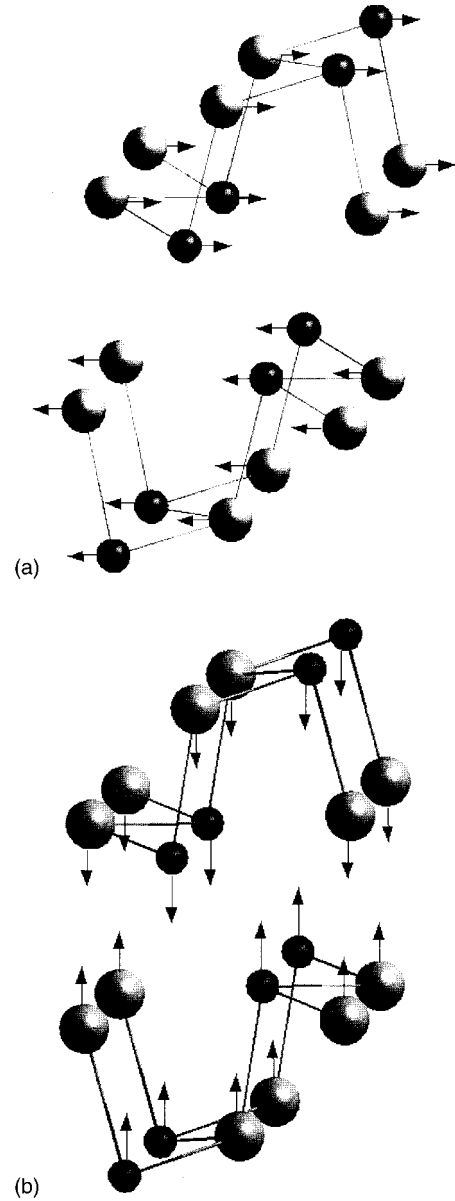
FIG. 7. Schematic illustration of the calculated eigenvectors corresponding to the (a) A_g shear mode and (b) B_{2g} compressive mode vibrations as determined by dynamical matrix diagonalization at ambient pressure. It is evident that the rigid-layer mode approximation is satisfied under ambient pressure conditions. The behavior of the eigenvectors under the point group symmetry operations of the structure were used to assign symmetry labels to the vibrations as described in more detail in the text.

2. Lattice dynamical response to hydrostatic pressure

The matrix diagonalization method and mode assignment procedure were repeated at several points along the hydrostatic line. We were thus able to obtain the pressure variation of both mode frequencies and displacement patterns. We also performed Raman scattering measurements up to a hydrostatic pressure of 64.8 kbar and room temperature.

In Figs. 9 and 10 we show the results of the experiment and calculation of the frequency response to pressure for several vibrations. In several of the spectra, the low-frequency region is complicated by the presence of a small
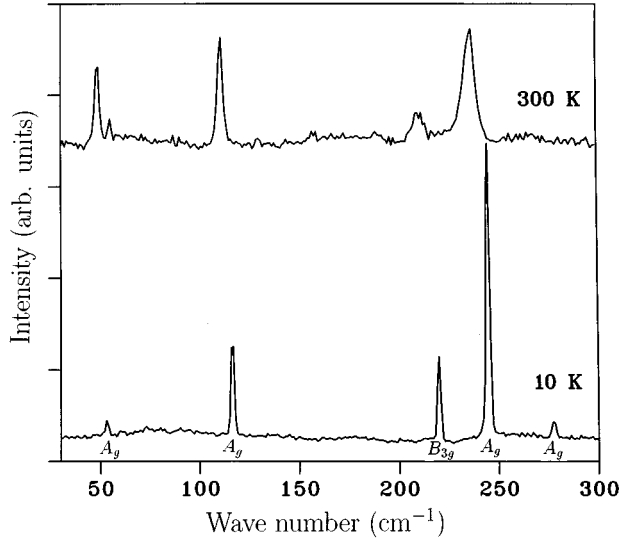
FIG. 8. Raman spectra of GeS at room temperature and 10 K. The count time was 20 sec per data point for both spectra. The observed difference in mode frequencies for the two temperatures is given in Table II along with the results from previous Raman spectroscopy studies of GeS.

amount of residual air contamination. Nevertheless the A_g shear mode is clearly visible at all pressures. However, the pressure evolution of the much weaker B_{3g} shear mode cannot be determined reliably as it is partially obscured by the strongest air line which is located at 60 cm^{-1}.

In the higher-frequency regime, it is evident that the calculated mode frequencies generally overestimate the experimental values although the overall degree of agreement between experiment and theory is quite good over the entire pressure range. It must be emphasized that the high-pressure experimental points have been obtained at room temperature

while the calculated points correspond to $T=0$. From Table II it is clear that the high-frequency modes are sensitive to temperature and do increase with decreasing temperature. In Fig. 10, we also include our low-temperature Raman data at ambient pressure. It would be of interest to perform the pressure-Raman experiments at low temperature.

At higher pressures, a pronounced sublinear pressure response of the RL A_g mode is found to occur[16] and this feature has been observed in Raman scattering studies of other layered compounds such as MoS$_2$ (Ref. 11) and As$_2$S$_3$.[38] The calculated frequency of this mode agrees well with the experimental values over the entire pressure range and it is clear that the dynamical matrix technique provides an accurate description of this vibration. By contrast, and as in the case with GeSe, the frozen-phonon calculation of this mode overestimates the frequency of this vibration and this overestimate becomes more severe with increasing pressure. In Fig. 10, the overestimate of the calculated frozen-phonon frequency of the lowest A_g shear mode is 17% higher than the experimental result at ambient pressure and reaches 24% by 50 kbar. We therefore assume that the rigid-layer approximation upon which the frozen-phonon calculation is based must not be valid at high pressures.

The pressure-induced changes of the lowest calculated shear and compressive mode eigenvectors demonstrate most clearly the breakdown of the rigid-layer mode behavior, as illustrated in Table III. The c and the a components of the eigenvectors of A_g and B_{2g} modes, respectively, are seen to increase with pressure. In Fig. 11 we show the displacement pattern of the lowest-frequency A_g and B_{2g} modes which clearly no longer display the simple rigid layer character which they did under ambient pressure conditions.

The pressure response of all low- to mid-frequency zone-center optical modes is shown along with their symmetry labels in Fig. 12. It is evident that Raman-infrared splittings

TABLE II. Frequencies of Raman-active phonons for GeS at room temperature and low temperature. The frequencies are given in units of cm^{-1}. In the first column we give the mode type. In the "symmetry" column we give the group assignments. The calculated mode frequencies shown in the last column are determined from diagonalization of the dynamical matrix by the method described in the text.

Description	Symmetry	ω_i (300 K)	ω_i (low T)	ω_i (calc.)
RL type	A_g	48,[a] 49,[b] 48[c]	51.5,[b] 52[c]	52.3
	B_{3g}	55,[a] 56,[b] 56[c]	58.5[b]	64.0
	B_{2g}	76,[a] 75[b]	76.5[b]	77.5
Bond-bending type	B_{1g}	96,[a] 94[b]	97[b]	94.5
	A_g	111,[a] 112,[b] 112[c]	115.5,[b] 116[c]	110.2
	B_{2g}	132,[a] 130[b]	133.5[b]	133.1
Bond-stretch type	B_{3g}	212,[a] 213,[b] 212[c]	219.5,[b] 219[c]	222.6
	A_g	238,[a] 239,[b] 238[c]	245.0,[b] 244[c]	241.4
	B_{1g}	215,[a] 245[b]	251[b]	249.8
	A_g	269,[a] 269,[b]	278.0,[b] 276[c]	280.7
	B_{2g}	242,[a] 281[b]	290[b]	287.7
	B_{2g}	329[b]	335.5[b]	318.6

[a]Reference 37.
[b]Reference 36.
[c]Present work.
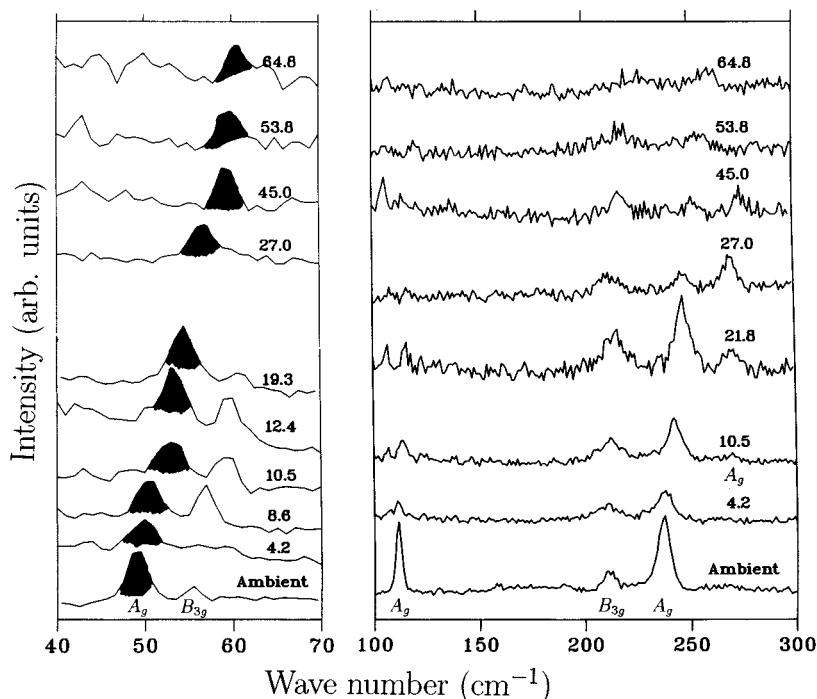
FIG. 9. Evolution with pressure of the room temperature Raman spectrum of GeS up to 64.8 kbar. The A_g shear mode is shown shaded. The weaker B_{3g} shear mode, while accessible in our $c(XY)\overline{c}$ scattering geometry, is obscured by the presence of residual air contamination and its response to pressure cannot be followed reliably in these measurements. Also, the low-frequency modes at 21.8 kbar were badly contaminated by air signals; we have therefore ommited these data points.

all increase with pressure indicating an enhanced interlayer interaction. Most dramatically, however, is the fact that by 50 kbar, the frequency of the B_{2g} shear mode increases to a value which is higher than that of three intralayer bond-bending vibrations. The point of crossover represents the complete loss of two-dimensional character of the vibrations. However, well before this point, examination of the eigenvectors reveals that the rigid-layer mode approximation has broken down.

VI. DISCUSSION

In this section we draw together the available results on the structural and vibrational properties in order to develop a comprehensive picture of pressure effects in this representative layered compound. We first concentrate on the compression mechanism of the GeS structure. Examination of the calculated pressure response of the cell and internal positional parameters of GeS reveals a strong similarity between the compression mechanism of this material and the isostructural compound GeSe. The main point for the following discussion is that the structure remains anisotropic up to pressures above 50 kbar. Comparison with experiment demonstrates that the compression mechanism of these compounds can be simulated reliably by first-principles calculation. It is particularly important to establish the accuracy with which quantum mechanical simulations can account for the compression mechanism if the simulation techniques are to be extended in order to study the pressure response of the vibrational properties.

The vibrations can be divided naturally into several regimes according to the degree of coupling between the layers. In the limiting regime of zero coupling between layers, the vibrations are described by diperiodic group symmetry and degeneracies exist between the Raman and infrared modes. No rigid-layer modes exist. Of course, this situation is never realized in the real material. At ambient pressure, splittings develop between the Raman and infrared modes and these splittings provide a measure of the interaction between layers. Somewhat surprisingly, the gap between the highest-frequency RL mode and the lowest-frequency intralayer bond-bending mode is only 10 cm^{-1} which is comparable to the separation between RL modes. This result indicates that even under ambient conditions, the vibrational properties are not as anisotropic as the structure might suggest. The previous estimates for the intralayer-intralayer force constant ratio[6] also showed the GeS is less anisotropic than other layered materials, such as graphite and As$_2$S$_3$.[1] Nevertheless the lowest-frequency vibrations are still well described by the rigid-layer approximation. Thus the ambient pressure situation corresponds to a weak-coupling regime. We should also note that the displacement pattern corresponding to infrared active vibrations may involve long-range dipolar forces which are not included in our calculations but which may affect the calculated infrared frequencies. It would be of interest to apply the density functional perturbation technique developed by Giannozzi et al.[39] to address this issue. Since Raman active modes are symmetric with respect to inversion, we expect these modes will not be affected by dipolar forces. This is supported by the excellent agreement we obtain between calculated and experimentally determined Raman-active mode frequencies.

At the relatively modest compressions, an intermediate regime exists in which the infrared and Raman splittings increase relative to their values at ambient pressure and all modes preserve their original relative position in order of increasing frequency. However, at this pressure, and unlike the weak-coupling case, it is evident that the lowest-frequency modes are no longer of pure rigid-layer character. The pressure-induced crossover from the weak to the inter-
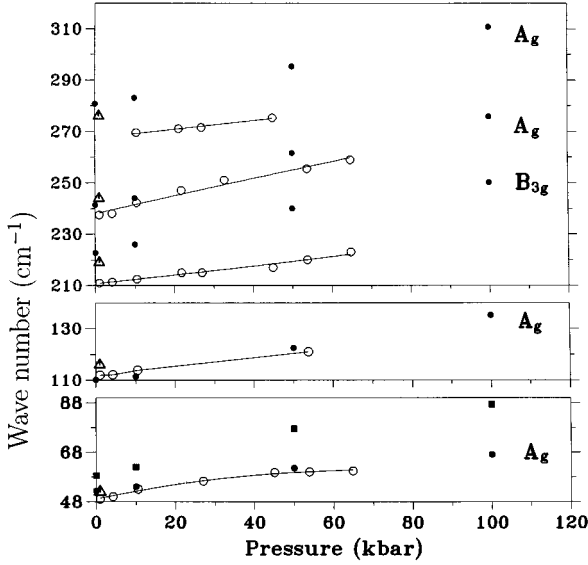
FIG. 10. The frequencies of the experimentally observed Raman modes as a function of pressure are shown as open circles. The solid curves through the data points are guides to the eye. The open triangles correspond to our 10 K measurements at ambient pressure. The corresponding mode frequencies vs hydrostatic compression as calculated by diagonalization of a dynamical matrix constructed from Hellmann-Feynman forces are shown as solid circles. It is clear that the temperature effect substantially improves the agreement between experimental and calculated phonon frequencies especially for the high-frequency modes. The results of the frozen-phonon calculation for the RL A_g shear mode are shown as solid squares. The frozen-phonon result overestimates the experimental frequencies and this overestimate becomes more severe with increasing pressure.

mediate coupling regime is gradual and is unlikely to be easily detected in spectroscopic studies since these provide no direct eigenvector information. It may be that the onset of sublinear pressure response of the rigid-layer modes is the spectroscopic signature of this crossover but more extensive simulations at closely spaced pressure intervals would be necessary to explore this. In view of the extreme computa-

tional cost of these calculations, we have not considered this possibility further in this work.

By 50 kbar, the relative position of the modes is substantially disrupted relative to that obtained at ambient pressure or 10 kbar. Significantly, this reordering of the relative positions removes the gap between interlayer and intralayer mode frequencies. Also the mode eigenvectors indicate a substantial breakdown of rigid-layer mode character at this pressure. This is therefore the strong-coupling regime in which the two-dimensional character of the vibrational properties is lost.

These results suggest that despite the fact that the crystallographic structure remains stable and highly anisotropic up to at least 94 kbar, the vibrational properties undergo a series of subtle, continuous modifications under compression. These modifications are unexpected on the basis of structural considerations alone. It may be that in more highly anisotropic solids, the RL mode approximation remains valid to higher pressures but we expect eventual breakdown to occur in all layered solids.

It is clear therefore that an accurate theoretical description of the lattice dynamical properties of layered solids over a wide pressure range is a challenging problem. In order to extract accurate phonon frequencies, it is essential to obtain a well-relaxed structure such that displacements which are small enough to be within the harmonic regime also give a measurable restoring force.

VII. CONCLUSIONS

In this paper, the pressure-induced structural and vibrational properties of the layered compound GeS have been extensively studied using a combination of theoretical and experimental methods. We have reported the response to hydrostatic pressure of the double-layered structure of GeS by using angle-dispersive powder x-ray diffraction and the results compared favorably with those of *ab initio* simulation. As in the case of GeSe, GeS has no structural phase transition up to at least 94 kbar. We have also considered the pressure effects on the vibrational properties of GeS by employing high-resolution pressure-Raman spectroscopy and a first-principles dynamical matrix scheme.

TABLE III. Calculated normalized eigenvectors of the A_g shear mode and B_{2g} compressive mode normal to the crystallographic b axis at several pressures. Ge_1 and S_1 are located on one double layer whereas Ge_2 and S_2 are located symmetrically on another double layer in the unit cell. Note the relatively large increase in the c and the a component of the displacements of A_g and B_{2g} mode, respectively, with increasing pressure indicating the breakdown of the RL approximation.

		Ge_1		Ge_2		S_1		S_2	
Symmetry	Pressure	a	c	a	c	a	c	a	c
A_g	Ambient	−0.42	0.11	0.42	−0.11	−0.24	0.00	0.24	0.00
	10 kbar	−0.42	0.13	0.42	−0.13	−0.23	0.01	0.23	0.01
	50 kbar	−0.42	0.19	0.42	−0.19	−0.20	0.02	0.20	0.02
	100 kbar	−0.42	0.20	0.42	−0.20	−0.17	0.04	0.17	0.04
B_{2g}	Ambient	−0.03	0.43	0.03	0.43	−0.01	0.25	0.01	0.25
	10 kbar	−0.04	0.43	0.04	0.43	−0.01	0.24	0.01	0.24
	50 kbar	−0.11	0.44	0.11	0.44	−0.03	0.22	0.03	0.22
	100 kbar	−0.34	0.32	0.34	0.32	−0.11	0.14	0.11	0.14
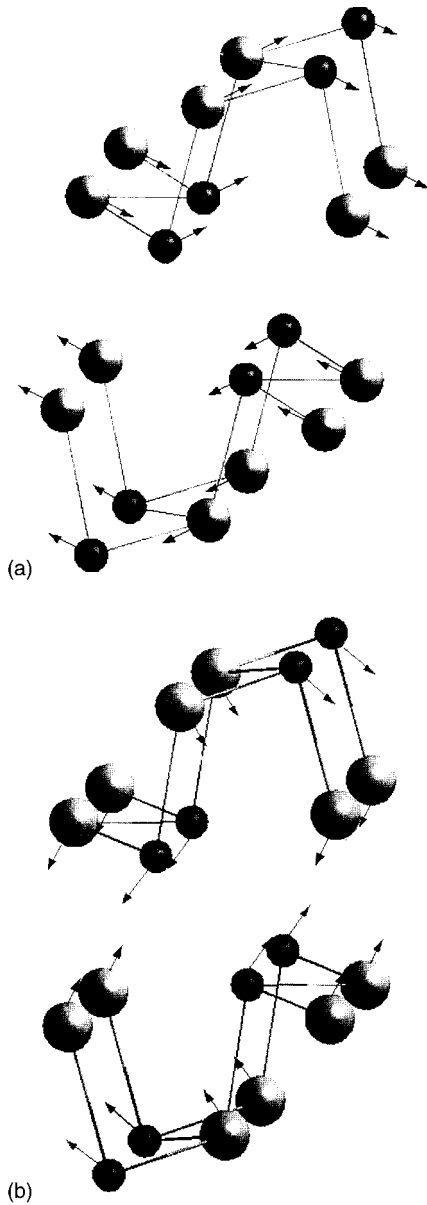
FIG. 11. Calculated eigenvectors corresponding to the (a) shear mode and (b) compressive mode vibrations as determined by dynamical matrix diagonalization at a pressure of 50 kbar. The displacement patterns at this pressure are clearly not of rigid-layer character.

FIG. 12. Calculated frequency and symmetry assignments at ambient and elevated pressure. The DG symmetry assignments are also shown and are included to identify the modes which would be degenerate in the absence of interlayer coupling. The frequency axis is therefore not appropriate for the DG assignments. It is evident that the splitting between Raman and infrared doublets increases with increasing pressure which is indicative of enhanced interlayer interaction. The infrared-active B_{3u} mode and the inactive A_u modes soften with pressure. By 50 kbar, there is no longer a gap in the calculated frequency between intralayer and interlayer vibrations which implies that two-dimensional character of the vibrational properties has been lost despite the fact the crystallographic structure remains highly anisotropic. We make no attempt to determine precisely the pressure at which this crossover occurs.

We find that the rigid-layer mode approximation is appropriate only near ambient pressure and only modest compression induces a breakdown of the rigid-layer displacement pattern. This provides an explanation for the failure of frozen-phonon calculations to account for the pressure response of the RL mode frequencies in layered materials. The calculated eigenvectors indicate the mode mixing of low-frequency vibration occurs continuously in response to pressure. We believe that pressure-induced breakdown of the rigid-layer mode approximation is not unique to GeS and GeSe and that it is expected to occur in any layered solid under compression. It will therefore be particularly interesting to apply the methods outlined in this paper to other layered materials such as MoS_2.

[1] R. Zallen and M. Slade, Phys. Rev. B **9**, 1627 (1974).

[2] E.A. Wood, Bell Syst. Technol. J. **43**, 541 (1964).

[3] R. Zallen, M.L. Slade, and A.T. Ward, Phys. Rev. B **3**, 4257 (1971).

[4] B.A. Weinstein and R. Zallen, in *Light Scattering in Solids IV*, edited by M. Cardona and G. Güntherodt (Springer-Verlag, Berlin, 1984), p. 463.

[5] J.L. Verble and T.J. Wieting, Phys. Rev. Lett. **25**, 362 (1970).

[6] J.D. Wiley, W.J. Buckel, and R.L. Schmidt, Phys. Rev. B **13**, 2489 (1976).

[7] N. Wakabayashi and R.M. Ni, in *Electrons and Phonons in Layered Crystal Structures*, edited by T.J. Wieting and M. Schlüter (Reidel, Dordrecht, Holland, 1979), p. 409.

[8] W. Kress, A. Frey, B. Dorner, and W. Kaiser, *Proceedings of the Conference on Neutron Scattering*, Catlinburg, TN, 1976 (US Dept. Commerce, Springfield, VA, 1976), Pt. I, p. 216.

[9] T.J. Wieting, Solid State Commun. **12**, 931 (1973).

[10] K. Allahverdi, S. Babaev, S. Ellialtioglu, and A. Ismailov, Solid State Commun. **87**, 675 (1993).

[11] S. Sugai and T. Ueda, Phys. Rev. B **26**, 6554 (1982).

[12] H.R. Chandrasekhar, R.G. Humphreys, U. Zwick, and M. Cardona, Phys. Rev. B **15**, 2177 (1977).

[13] R. Zallen, Phys. Rev. B **9**, 4485 (1974).

[14] H.C. Hsueh, H. Vass, S.J. Clark, G.J. Ackland, and J. Crain, Phys. Rev. B **51**, 16 750 (1995).

[15] K.L. Bhatia, G. Parthasarathy, D.P. Gosain, and E.S.R. Gopal, Phys. Rev. B **33**, 1492 (1986).

[16] H.C. Hsueh, H. Vass, S.J. Clark, and J. Crain, Europhys. Lett. **31**, 151 (1995).

[17] Ralph W.G. Wyckoff, *Crystal Structures*, 2nd ed. (Wiley, New York, 1963), Vol. 1, p. 102.

[18] R.J. Nelmes and M.I. McMahon, J. Synchrotron Radiat. **1**, 69 (1994).

[19] R.O. Piltz, M.I. McMahon, J. Crain, P.D. Hatton, R.J. Nelmes, R.J. Cernik, and G. Bushnell-Wye, Rev. Sci. Instrum. **63**, 700 (1992).

[20] A.N. Fitch, J.K. Cockcroft, and A.D. Murray (unpublished).

[21] J.P. Perdew and A. Zunger, Phys. Rev. B **23**, 5048 (1981).

[22] L. Kleinman and D.M. Bylander, Phys. Rev. Lett. **48**, 1425 (1982).

[23] J.S. Lin, A. Qteish, M.C. Payne, and V. Heine, Phys. Rev. B **47**, 4147 (1993).

[24] M.H. Lee, J.S. Lin, M.C. Payne, V. Heine, V. Milman, and S. Crampin (unpublished).

[25] H.J. Monkhurst and J.D. Pack, Phys. Rev. B **13**, 5188 (1976).

[26] R.M. Wentzcovitch, Phys. Rev. B **44**, 2358 (1991).

[27] M. Parrinello and A. Rahman, Phys. Rev. Lett. **45**, 1196 (1980).

[28] P. Gomes Dacosta, O.H. Nielsen, and K. Kunc, J. Phys. C **19**, 3163 (1986).

[29] P. Pulay, Mol. Phys. **17**, 197 (1969).

[30] G.P. Francis and M.C. Payne, J. Phys. Condens. Matter **2**, 4395 (1990).

[31] A.A. Maradudin, E.W. Montroll, G.H. Weiss, and I.P. Ipatova, *The Theory of Lattice Dynamics in the Harmonic Approximation*, Solid State Physics Supplement Vol. 3, 2nd ed. (Academic, New York, 1971).

[32] Since the displaced configuration is of lower symmetry than the equilibrium configuration it is necessary to regenerate the Monkhorst-Pack k-point set for the displaced configuration. This is done to preserve the Brillouin zone sampling density. The dynamical matrix construction is thus performed with a 16 special k-point set for displacements along the a and c directions and a 32 k-point set for displacement along the b direction as opposed to the 8 special k-point set which was used to determine the equilibrium structure.

[33] T. Chattopadhyay, A. Werner, and H.G. von Schnering, in *High Pressure in Science and Technology*, edited by C. Homan, R.K. MacCrone, and E. Whalley, MRS Symposia Procedings No. 22 (Materials Research Society, Pittsburgh, 1984).

[34] G. Burns and A.M. Glazer, *Space Groups for Solid State Scientists* (Academic, New York, 1978).

[35] For example, we applied eight symmetry operations (including one identity, three twofold rotations about the principal axis, one inversion, and three reflections about planes normal to the principal axis) of the point group $mmm(D_{2h})$ to the eigenvector of the lowest-frequency vibration and then we determined that the eigenvector is symmetric under each symmetry operation. Thus the character for each symmetry operation is $+1$. According to the character table of point group $mmm(D_{2h})$, we assigned this phonon to A_g symmetry. The assignments of the other modes can be decided by the same procedure.

[36] V. Vorlicek, I. Gregora, and D. Chvostova, Phys. Status Solidi B **116**, 639 (1983).

[37] H.R. Chandrasekhar, R.G. Humphreys, and M. Cardona, Phys. Rev. B **16**, 2981 (1977).

[38] J.M. Besson, J. Cernogora, and R. Zallen, Phys. Rev. B **22**, 3866 (1980).

[39] P. Giannozzi, S. de Gironcoli, P. Pavone, and S. Baroni, Phys. Rev. B **43**, 7231 (1991).

[40] T. Grandke and L. Ley, Phys. Rev. B **16**, 832 (1977).